

Refractive Index Sensing and Label-Free Detection Employing Oval Resonator Structured Plasmonic Sensor

A. Harhouz^{1,*}, A. Hocini^{1,†}, H. Tayoub^{1,2,‡}

¹ *Laboratoire d'Analyse des Signaux et Systèmes, Department of Electronics, University of MSila, P.O. BOX. 166, Route Ichebilja, Msila 28000, Algeria*

² *Research Center in Industrial Technologies CRTI, P.O. BOX. 64, Cheraga 16014, Algiers, Algeria*

(Received 21 January 2022; revised manuscript received 20 February 2022; published online 28 February 2022)

Plasmonics is a young area of nano-optics research. Owing to its ability to produce nanoscale hot spots, which are close to the size of bioparticles, it has been largely applied in biodetection with enhanced matter/light interactions and heightened sensitivity to refractive index (RI) changes. In this manuscript, we propose a miniature plasmonic RI sensor with high detection performances. Our proposed plasmonic RI sensor based on Fano resonances in a metal-insulator-metal (MIM) waveguide with a nanowall coupled with an oval resonator is presented in this work. The spectral characteristics and the transmission properties of the sensor are extensively analyzed using the finite difference time-domain (FDTD) method. The proposed sensor proves to be highly sensitive for label-free detection with an optimum design. FDTD simulations show that RI sensitivity values can be as high as 3787.9 nm per refractive index unit (RIU).

Keywords: Fano resonance, Plasmonic RI sensor, MIM waveguide, FDTD, Oval resonator.

DOI: [10.21272/jnep.14\(1\).01012](https://doi.org/10.21272/jnep.14(1).01012)

PACS number: 42.81.Pa

1. INTRODUCTION

With the fast development of nanofabrication skills, nano-optics has been applied and improved in several areas of research and industry. One major branch of nano-optics is plasmonic sensing. Owing to its ability to create nanoscale hot spots, which are close to the size of bioparticles, plasmonics has been widely applied in biosensing with improved light/matter interactions and enhanced sensitivity to refractive index (RI) variations [1-6].

The modern plasmonic sensor industry is faced with the search for new nanostructures with design functions, where the concept of utilizing surface plasmon polaritons (SPPs) proves itself useful over other nanotechnologies. SPPs are guided electromagnetic waves that propagate along the metal-insulator interface due to the ability to modulate light on the nanoscale, as well as break the diffraction limit, which has been widely discussed for several decades [7, 8]. One of the basic plasmonic waveguides capable of confining light within a considerable propagation length is the metal-insulator-metal (MIM) waveguide [9], and several studies of RI sensors are based on this structure [10-14]. For example, Zhang et al. [12] proposed a plasmonic RI nanosensor based on MIM waveguide-coupled double rectangular cavities, which can achieve an RI sensitivity (S) of 596 nm/RIU and a figure of merit (FOM) of 7.5. A plasmonic waveguide coupled system that uses a MIM waveguide with two silver baffles and a coupled ring cavity was shown by Zhao et al. [15] with an S of 718 nm/RIU. Zhang et al. [16] also presented a symmetric plasmonic waveguide with a shoulder-coupled rectangle cavity that has an FOM of 57. As an RI sensor, it requires both high FOM and high sensitivity (S)

to assure excellent performance. Currently, Fano resonance is generally used to improve FOM that results from structural symmetry breaking or dark-bright resonance interference and has an asymmetric spectral line shape with a narrower full width at half maximum (FWHM) [12, 14, 15, 17].

In this context, a highly sensitive plasmonic RI sensor based on Fano resonances in a MIM waveguide coupled with a defective oval resonator is proposed. The transmission properties are numerically simulated by finite-difference time-domain (FDTD) method. The properties of the proposed structure in applications of RI sensing are studied in detail, which shows that the designed plasmonic system can have promising applications for integrated optical devices of nanoscale optical switches, sensors, and optical filters.

2. DESIGN AND THEORETICAL ANALYSIS

The proposed structure of the plasmonic RI sensor is schematically shown in Fig. 1. It consists of an MIM waveguide coupled with a thin metal nanowall directly below a defective oval resonator. Throughout this work, the width of the MIM waveguide is fixed as $w = 50$ nm [18] to ensure that only the fundamental TM₀ type SPP mode can be excited and transmitted.

The MIM waveguide is coupled with a side defective oval resonator above the nanowall, with R as the radius of two intertwined disks with distance X_R , the nanowall thickness is D . The green and white areas represent the silver layer ϵ_m and the dielectric material ϵ_{in} , respectively. In all simulations performed in this work using FDTD, the Debye-Drude dispersion model [19-21] can describe the relative permittivity of silver:

* ahlam.harhouz@univ-msila.dz

† abdesselam.hocini@univ-msila.dz

‡ hadjira.tayoub@univ-msila.dz

$$\varepsilon_m(\omega) = \varepsilon_\infty - \frac{\omega_p^2}{\omega(\omega + i\gamma)},$$

where $\omega = c/\lambda$ is the incident SPP frequency, ε_∞ is the dielectric constant at an infinite angular frequency with a value of 3.7, $\omega_p = 1.38 \cdot 10^{16}$ Hz is the bulk plasma frequency, ω is the incident wave frequency, $\gamma = 2.73 \cdot 10^{13}$ Hz is the electron collision frequency.

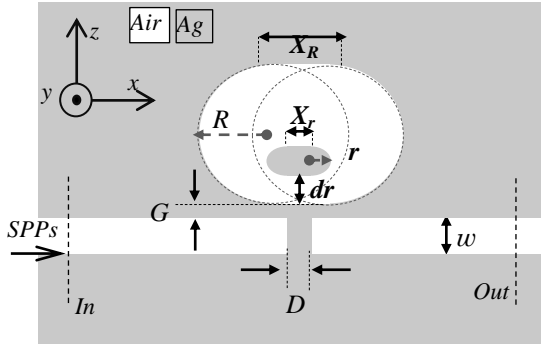


Fig. 1 – Proposed design. The geometric parameters of the proposed structure were set as follows: $w = 50$ nm, $D = 50$ nm, $R = 300$ nm, $X_R = 80$ nm, $r = 40$ nm, $X_r = 60$ nm, $g = 10$ nm

In our simulation, the spectral responses of the designed plasmonic structure are numerically studied by the 2D FDTD method using the commercial simulator R-Soft. During the simulation, it is supposed that the thickness of the Y direction is infinite, and for a real 3D structure in the laboratory, this supposition is acceptable for thicknesses larger than $1 \mu\text{m}$ [22, 23]. In our study, only the 2D model is investigated, and this is to consider the trade-off between computational accuracy and time costs. Perfectly matched layer (PML) boundary conditions are used in FDTD simulations, and a uniform mesh grid ($\Delta x, \Delta z$) equal to 5 nm was chosen to ensure speed and accuracy of the calculation in both x and z directions [24]. The Gaussian light source is placed on the left side of the waveguide. When the incident light is a TM-polarized wave, SPPs will be excited, confined and transmitted in the waveguide. When the transmitted light is collected from the right side of the waveguide, the transmittance T can be calculated as follows [14, 25]:

$$T = \frac{P_{out}}{P_{in}}, \quad (2)$$

where P_{in} and P_{out} are the incident power and the transmitted power observed at positions A and B, respectively.

3. NUMERICAL SIMULATION, RESULTS AND DISCUSSION

There are many topologies for designing optical sensors based on the plasmonic structure. These optical sensors usually include waveguides and resonators. In this work, a simple structure of an RI sensor with high detection parameters is designed. The simulation results due to the interaction of incident waves with the designed RI sensor are presented. The geometric parameters of the proposed design are set as: $w = 50$ nm,

$D = 50$ nm, $R = 300$ nm, $X_R = 80$ nm, $r = 40$ nm, $X_r = 60$ nm, $d_r = 160$ nm, $g = 10$ nm. The simulated transmission spectra are numerically calculated by the FDTD method and presented in Fig. 2.

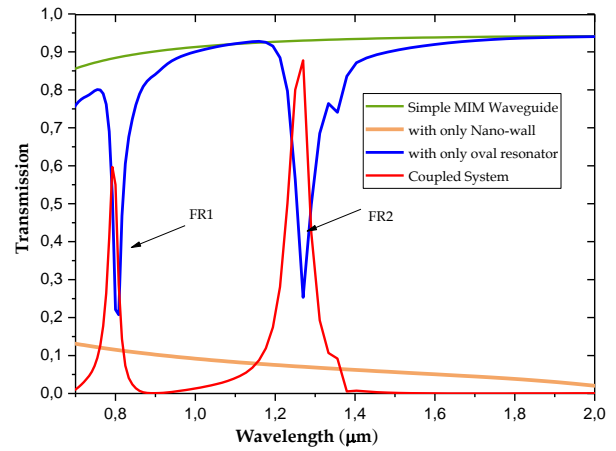


Fig. 2 – FDTD simulation results. Transmission spectra of a simple MIM waveguide, a MIM waveguide with only a nanowall, a MIM waveguide with only a defective oval resonator, and a coupled system (a MIM waveguide with a nanowall side-coupled to the oval resonator)

The transmission spectra of a simple MIM waveguide are greater than 0.8 in the range of 700-200 nm (green curve in Fig. 2). For a MIM waveguide with a metal nanowall, the transmittance (orange curve) is less than 0.16 in the same range. Here, the spectrum can be considered as a wide continuum state, this is due to the nanowall, which practically blocks the transmission. To create a discrete state, a defective oval cavity is side coupled with the MIM waveguide. It can be seen clearly that in the range of 700-1500 nm, there are two symmetric Lorentzian-like valleys, which represent the first and second modes of the defective oval cavity, and this can be regarded as two discrete states. When the nanowall is inserted into a MIM waveguide and coupled with a defective oval resonator, interference will occur between two states, one continuum and one discrete, thus two sharp and asymmetric Fano resonances will appear in the transmission spectrum (red curve). Fano resonance peaks are marked by FR1 and FR2 with wavelengths $\lambda_{FR1} = 792.079$ nm and $\lambda_{FR2} = 1269.84$ nm.

Two Fano resonances can be tuned by the geometric parameters of a defective resonator or a metal nanowall. For the first time, the effect of the radii R and r on the transmission spectra is studied and displayed in Fig. 3a.

Here, the other geometric parameters are the same as above in the simulation calculation. A wavelength shift of the Fano peaks is observed when the radius R of two intertwined disks increases from 290 to 330 nm with a step of 10 nm. The position of the Fano peaks is directly affected by the position of the resonant modes of the oval resonator. In addition, this is because the proposed Fano resonances are provided by two discrete states arising from the side coupled oval resonator. For a better understanding of the physical mechanism of the Fano resonance, the magnetic field distributions H_y

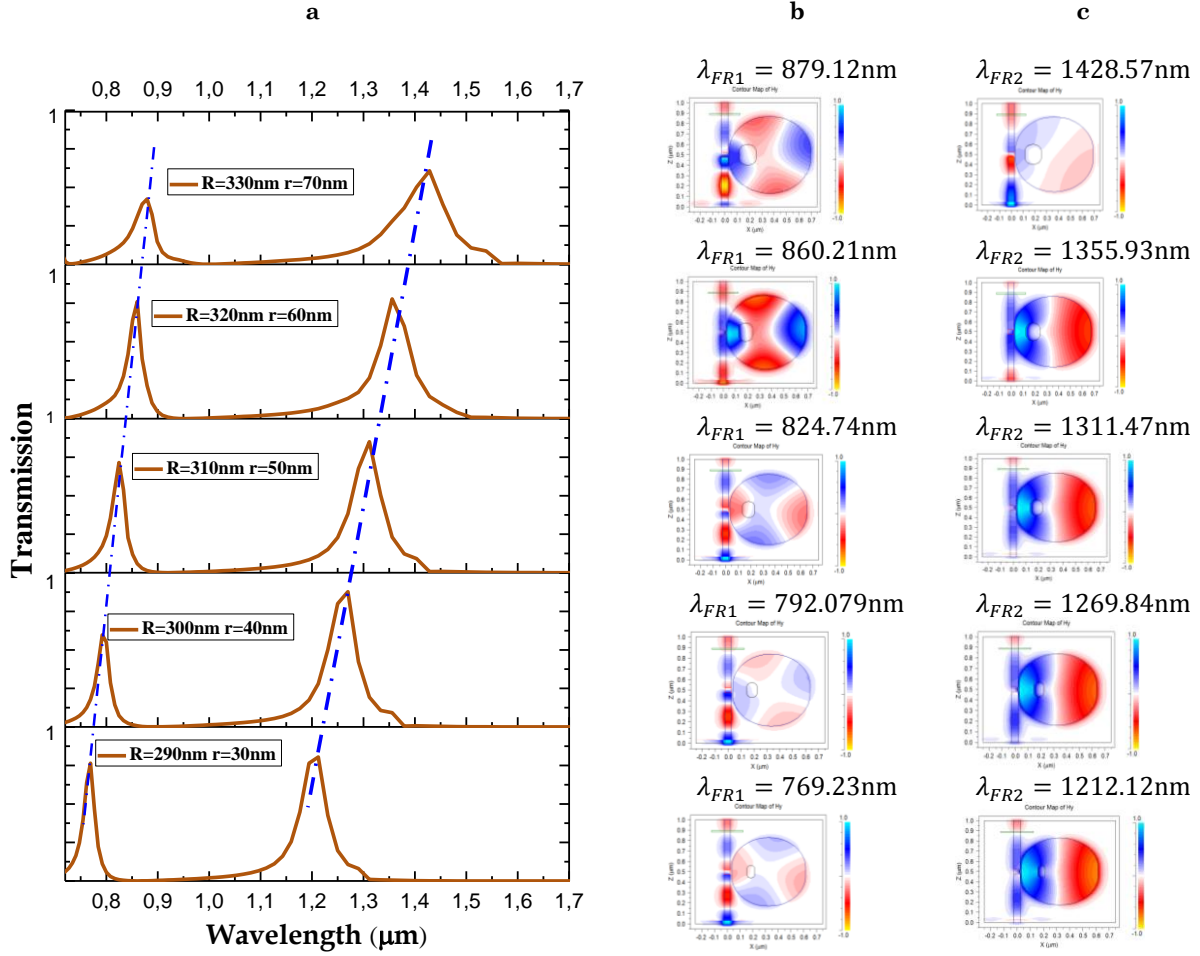


Fig. 3 – (a) Transmission spectra of the plasmonic Fano system with different radius R ; (b) and (c) magnetic field distributions (H_y) at two resonance wavelengths λ_{FR1} and λ_{FR2} , respectively, for radius R

at the wavelengths of the two transmission peaks λ_{FR1} and λ_{FR2} are presented in Fig. b and Fig. 3c, respectively (for different R). TM_m classifies the resonance modes, where m is the number of nodes of stationary waves in the defective oval resonator. From Fig. b and Fig. 3c, the resonant modes are TM_4 and TM_2 , respectively. It is also obvious that, at $R = 320\text{ nm}$, the electromagnetic wave energy is mainly confined in the defective oval resonator for two Fano resonance peaks. Therefore, these peaks are more sensitive to the alteration of RI around the distribution surface, which is very helpful for enhancing the sensitivity and performance of the biosensor. For the second time, we keep the previous parameters and analyze the transmission with the variation of the distance X_r of the inner oval. The effect of the distance X_r of the inner oval on the transmission spectra is studied and displayed in Fig. 4a, b. An increase in the value of X_r is associated with an increase in the resonance wavelength, meaning that the X_r value causes a shift in the resonance wavelength, and the shift for FR2 is larger than that for FR1 due to larger losses. At the same time, we studied the effect of this parameter on sensitivity (S), which is vital for sensors. It is characterized by the unit wavelength shift $\Delta\lambda$ of the unit RI change Δn [26, 27] and can be expressed as $S = \Delta\lambda/\Delta n$. In addition to S , another term used to evalu-

ate the performance of a plasmonic sensor is FOM, which can be expressed in terms of both S and FWHM of the resonance peak, i.e., $FOM = S/\text{FWHM}$ [28].

As we mentioned earlier, the electromagnetic wave energy is mainly confined in a defective oval resonator. Therefore, the peaks are sensitive to the alteration of RI around the distribution surface.

By varying the RI of the outer oval from $n = 1$ to $n = 1.02$, one can induce a shift of the resonance spectrum. From Fig. 4c, an enhancement of the sensor sensitivity is achieved by increasing the value of X_r to the maximum value at $X_r = 400\text{ nm}$, after which sensitivity decreases. For FR1, the maximum sensitivity value is $1081.81\text{ nm}/\text{RIU}$, while for FR2 it is $3787.9\text{ nm}/\text{RIU}$, i.e., sensing resolution of $9.24 \cdot 10^{-6}\text{ RIU}$ for FR1 and $2.63 \cdot 10^{-6}\text{ RIU}$ for FR2 is achieved at $X_r = 400\text{ nm}$.

Finally, the transmission spectra of the optimal proposed design with different RI are presented in Fig. 5. Also, Fig. 6 shows an approximately linear relationship between the resonance wavelengths of the two modes (FR1, FR2) and RI. Table 1 compares the sensitivity of different sensors previously reported. The high sensitivity value achieved with the proposed device opens up the avenues for designing real time on-chip optical plasmonic RI sensors.

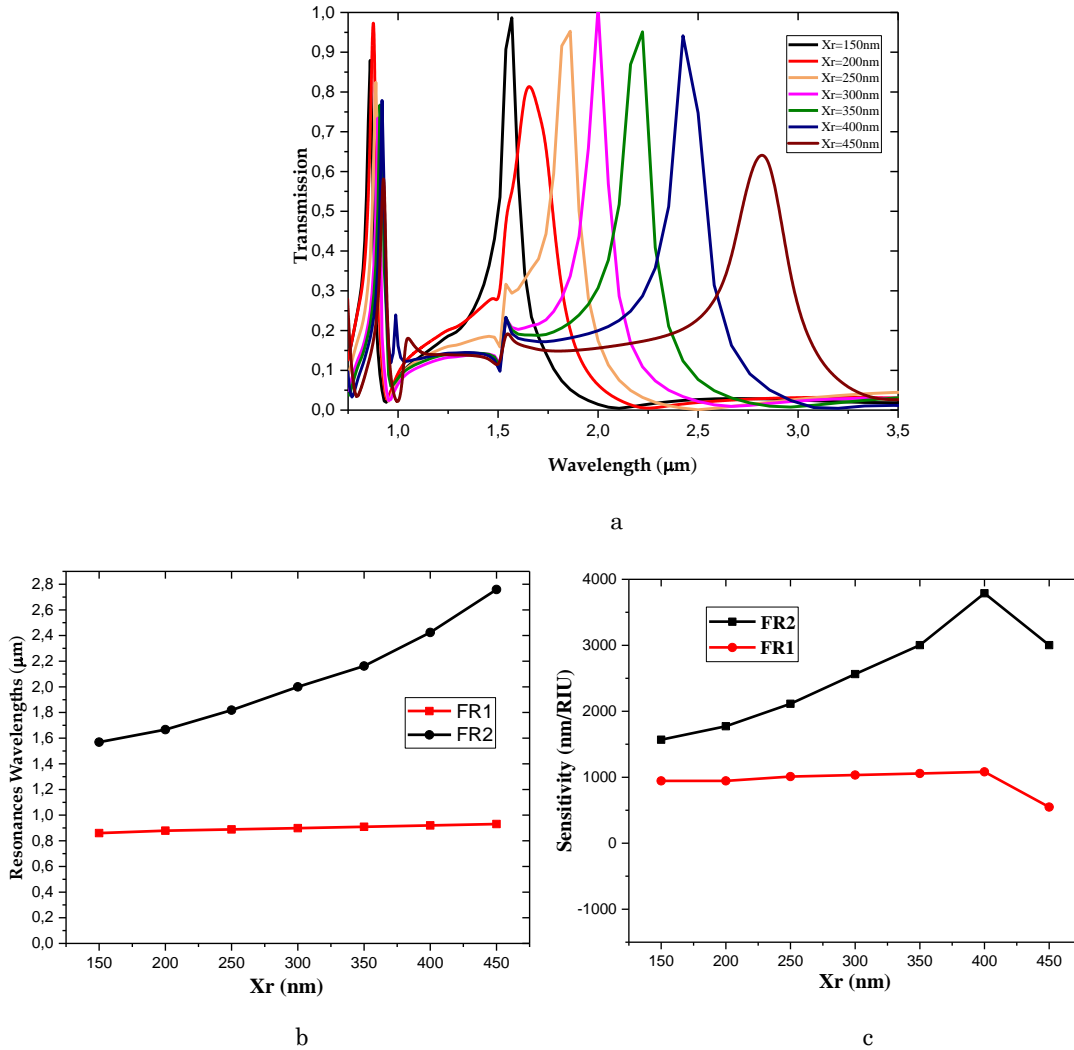


Fig. 4 – (a) Transmission spectra of the plasmonic Fano system with different distance X_r , (b) and (c) resonance wavelengths and sensitivities of the plasmonic sensors, respectively, for X_r varying from 150 to 450 nm

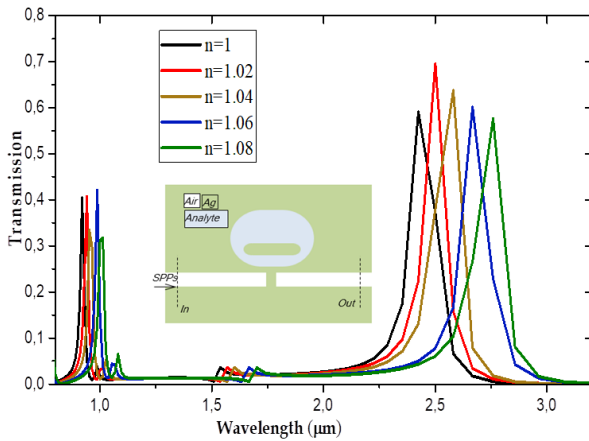


Fig. 5 – Transmission spectra of the plasmonic RI sensor with different RI

4. CONCLUSIONS

Transmission spectra of two Fano resonances can be formed by a combined plasmonic design made up of a MIM waveguide with a thin nanowall and a defective

oval resonator. The continuous state is supported by the MIM waveguide with the nanowall, whilst the defective oval resonator can create two discrete states. Coherent coupling and interference between the two states generate two Fano resonances. FDTD-based numerical simulations are performed to study the

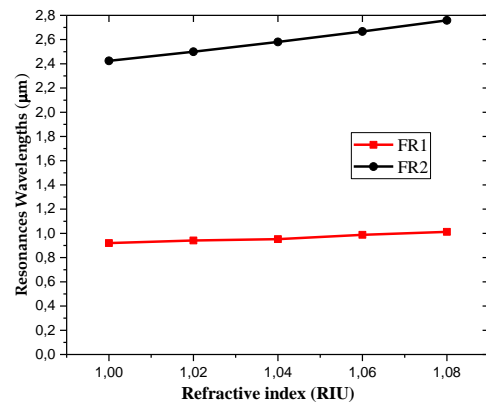


Fig. 6 – Resonance of plasmonic RI sensors for n varying from 1 to 1.08 nm

Table 1 – Sensitivity comparison of different sensor structures

References	Sensitivity (nm/RIU)
Yan et al. (2017) [29]	1071.4
Ghorbani et al. (2018) [30]	1540 for mode 2 and 1010 for mode 1
Bensalah et al. (2019) [24]	2602.5
Hocini et al. (2020) [6]	2448 for mode 2 and 1120 for mode 1
This work	3787.9 nm/RIU for FR2, 1081.81 nm/RIU for FR1

dependences of the transmission properties on the geometric parameters. As one of the potential applica-

tions, i.e., plasmonic RI sensor, the simulation results prove that the proposed sensor can achieve a high sensitivity of 3787.9 nm/RIU corresponding to the FR2 peak. Finally, this design, due to its small size, high sensitivity and high FOM, is very suitable for use in highly integrated circuits.

ACKNOWLEDGEMENTS

This work was supported by the Algerian Ministry of Higher Education and Scientific Research and La Direction Générale de la Recherche Scientifique et du Développement Technologique (DGRSDT) via funding through the PRFU Project No. A25N01UN280120180001.

REFERENCES

1. K. Agarwal, S. Hwang, A. Bartnik, N. Buchele, A. Mishra, J.-H. Cho, *Small* **14**, 1801145 (2018).
2. X. Yang, Z. Sun, T. Low, H. Hu, X. Guo, F.J. Garca de Abajo, P. Avouris, Q. Dai, *Adv. Mater.* **30**, 1704896 (2018).
3. J.R. Mejia-Salazar, O.N. Oliveira Jr, *Chemical Rev.* **118**, 10617 (2018).
4. A.B. Taylor, P. Zijlstra, *ACS Sensors* **2**, 1103 (2017).
5. S.E. Achi, A. Hocini, H.B. Salah, A. Harhouz, *Progress Electromagn. Res.* **96**, 147 (2020).
6. A. Hocini, H. Ben salah, D. Khedrouche, N. Melouki, *Opt. Quantum Electron.* **52**, 336 (2020).
7. W.L. Barnes, A. Dereux, T.W. Ebbesen, *Nature* **424**, 824 (2003).
8. G. Kumar, P.K. Sarswat, *Plasmonics*, 103 (Springer: 2016).
9. S.A. Maier, *Plasmonics: fundamentals and applications* (Springer Science and Business Media: 2007).
10. R. Zafar, M. Salim, *IEEE Sensors J.* **15**, 6313 (2015).
11. S.-B. Yan, L. Luo, C.-Y. Xue, Z.-D. Zhang, *Sensors* **15**, 29183 (2015)
12. Z. Zhang, L. Luo, C. Xue, W. Zhang, S. Yan, *Sensors* **16**, 642 (2016).
13. A. Harhouz, A. Hocini, *Opt. Quantum Electron.* **53**, 439 (2021).
14. Y. Tang, Z. Zhang, R. Wang, Z. Hai, C. Xue, W. Zhang, S. Yan, *Sensors* **17**, 784 (2017).
15. X. Zhao, Z. Zhang, S. Yan, *Sensors* **17**, 1494 (2017).
16. B.-H. Zhang, L.-L. Wang, H.-J. Li, X. Zhai, S.-X. Xia, *J. Optics* **18**, 065001 (2016).
17. J. Chen, Z. Li, Y. Zou, Z. Deng, J. Xiao, Q. Gong, *Plasmonics* **8** No 4, 1627 (2013).
18. H. Gai, J. Wang, Q. Tian, *Appl. Opt.* **46**, 2229 (2007).
19. H. Lu, X. Liu, D. Mao, Y. Gong, G. Wang, *Opt. Lett.* **36**, 3233 (2011).
20. X. Zhang, M. Shao, X. Zeng, *Sensors* **16**, 1730 (2016).
21. L. Dong, X. Xu, C. Li, Y. Guo, K. Sun, Y. Ding, *Opt. Commun.* **410**, 751 (2018).
22. Q. Wang, Z. Ouyang, M. Lin, Q. Liu, *Mater.* **11**, 1675 (2018).
23. F. Chen, H. Zhang, L. Sun, J. Li, C. Yu, *Opt. Laser Technol.* **116**, 293 (2019).
24. H. Ben salah, A. Hocini, M. Temmar, D. Khedrouche, *Chinese J. Phys.* **61**, 86 (2019).
25. X. Piao, S. Yu, S. Koo, K. Lee, N. Park, *Opt. Express* **19**, 10907 (2011).
26. Y. Wang, S. Li, Y. Zhang, L. Yu, *IEEE Photonics J.* **8**, 18 (2016).
27. Y. Zhang, S. Li, X. Zhang, Y. Chen, L. Wang, Y. Zhang, L. Yu, *Opt. Commun.* **370**, 203 (2016).
28. Y. Zhang, S. Li, Z. Chen, P. Jiang, R. Jiao, Y. Zhang, L. Wang, L. Yu, *Plasmonics* **12**, 1099 (2017).
29. S. Yan, M. Zhang, X. Zhao, Y. Zhang, J. Wang, W. Jin, *Sensors* **17**, 2879 (2017).
30. S. Ghorbani, M.A. Dashti, M. Jabbari, *Phys.* **28**, 066208 (2018).

Визначення показника заломлення та безмаркерне детектування з використанням структурованого плазмонного датчика з овальним резонатором

A. Harhouz¹, A. Hocini¹, H. Tayoub^{1,2}

¹ *Laboratoire d'Analyse des Signaux et Systèmes, Department of Electronics, University of MSila, P.O. BOX. 166, Route Ichebilia, Msila 28000, Algeria*

² *Research Center in Industrial Technologies CRTI, P.O. BOX. 64, Cheraga 16014, Algiers, Algeria*

Плазмоніка – молода область досліджень в галузі нанооптики. Завдяки здатності створювати нанорозмірні гарячі точки, які близькі до розміру біочастинок, вона широко застосовується в біодетектуванні з покращеною взаємодією речовина/світло та підвищеною чутливістю до змін показника заломлення (RI). У статті ми пропонуємо мініатюрний плазмонний датчик RI з високими характеристиками детектування. У роботі представлено запропонований нами плазмонний датчик RI на основі резонансів Фано у хвилеводі зі структурою метал-ізолятор-метал (MIM) з наностінкою, поєднаною з овальним резонатором. Спектральні характеристики та властивості пропускання датчика детально проаналізовані за допомогою методу кінцевих різниць у часовій області (FDTD). Запропонований датчик виявив високу чутливість до безмаркерного детектування при оптимальній конструкції. Моделювання FDTD показує, що значення чутливості за RI можуть досягати 3787,9 нм на одиницю показника заломлення (RIU).

Ключові слова: Резонанс Фано, Плазмонний датчик показника заломлення (RI), Хвилевод зі структурою MIM, FDTD, Овальний резонатор.